ISSN 2347-3487
Volume 12 Number 3
Journal of Advances in Physics

Study on anisotropies and momentum densities in AlN, GaN and InN by positron annihilation

N. Amrane, M. Benkraouda, N. Qamhieh, Saleh T. Mahmoud
Department of physics, U.A.E. University, Al-Ain, P.O. Box: 15551, U.A.E.
E-mail: namrane@uaeu.ac.ae

Abstract

The independent particle model (IPM) coupled with empirical pseudopotential method (EPM) was used to compute the thermalized positron charge densities in specific family of binary tetrahedrally coordinated crystals of formula A^NB^{8-N}. Initial results show a clear asymmetrical positron charge distribution relative to the bond center. It is observed that the positron density is maximum in the open interstices and is excluded not only, from the ion cores but also to a considerable degree from the valence bonds. Electron-positron momentum densities are calculated for the (001,110) planes. The results are used to analyze the positron effects in AlN, GaN and InN compounds. Our computational technique provides the theoretical means of interpreting the k-space densities obtained experimentally using the two-dimensional angular correlation of annihilation radiation (2D-ACAR).

I-INTRODUCTION

Positron annihilation experiments have been extensively used to investigate the electronic structure of pure metals, alloys and metals containing defects such as mono-vacancies, dislocations and large voids [1,2]. If the results of the experiments are to be used to obtain information about the electronic structure in these systems, it is important to have some knowledge of the spatial distribution of the annihilating positron [3].

Experiments and theory indicate that the measured two-photons angular correlation curves reflect the momentum space density of the electrons seen by injected positrons and contain information about the occupied regions of **k**-space [4,5], i.e. the Fermi surface [6]. The investigation of the electronic properties of solid by use of electronic and positronic charge densities represent an area of increasing importance. So far, most of the work has concerned electron charge densities as this has been found useful for the understanding of chemical bonds and recently for the modification of band structures by interstitial impurities [7,8]. The great success of recent developments in this field provokes us to ask for a better understanding of the charge densities. We will try to show that both electronic and positronic charge densities could provide complementary information about the structure of semiconductors.

On the theoretical side, there has been some attempt to study the behavior of the positron wave function in compound semiconductors and alloys. This paper reports a theoretical framework for calculating the distribution of thermalized positrons and the electron pseudo-charge density for GaN, InN and AlN compounds.

Gallium nitride (GaN) and Aluminum nitride (AlN) are two of the most promising III-V semiconductors for short wavelength optoelectronic devices [9,10]. The quest for light emitters and detectors operating from the blue to UV regions of the electromagnetic spectrum has tantalized researchers for several decades. Not long ago, most of the research work concentrated on the wide band gap II-VI materials ZnS and ZnSe with direct band gap structure. Lifetime problems and difficulties arising from the p-type doping have plagued effort on these materials. In the meantime, investigations have concentrated on the study of nitrides based III-V compounds. A lot of interest has been generated in the III-V nitrides because of the commercially available blue and green light emitting diodes based on an InGaN-GaN heterostructure [11]. The breakthrough of doping GaN via substitution of gallium by magnesium [12] and the fact that it is widely believed that self-compensation problems do not plague III-V semiconductors, and so the existence of the iso-anionic semiconductors InN, GaN and AlN with large band gap (2 eV (orange), 3.5 eV (ultraviolet), and 6 eV (ultraviolet), respectively), has raised the possibility of fabricating nitride based materials.

GaN is, by far, the most heavily studied of all of the III-V nitrides, yet, compared to Si and GaAs semiconductors, relatively little is known about GaN. The zinc blende GaN has a higher saturated electron drift velocity [13] and a somewhat lower energy band gap than wurtzite GaN. Mizuta et al. [14] first reported bulk zinc blende GaN grown on (001) GaAs. InN is, in the context of nitrides, probably the least known. InN has received the same attention as GaN and AlN primarily because the 1.9 eV band gap for InN corresponds to a portion of the electromagnetic spectrum in which alternative semiconductor technology exists. The band gap of this material is direct and the optical absorption threshold lies in the orange portion of the visible spectrum. This material has recently been synthesized in zinc blende structure [15] with a measured lattice constant of 0.498 nm.

Computational details are given in section 2, and section 3 is devoted to the discussion of the results.

II- FORMALISM

In the independent particle approximation [16-18], the probability of annihilation of the electron-positron pair with momentum **p** is given by:

$$\Gamma(\mathbf{p}) = const \sum_{n} \sum_{k}^{occ.} \left| \int_{\Omega} \psi_{n\mathbf{k}}(\mathbf{r}) \phi(\mathbf{r}) \exp(-i\mathbf{pr}) d\mathbf{r} \right|^2 \qquad (1)$$

where ψ_{nk} is the Bloch wave function of the valence electron with wave vector ***k*** in the n[th] band, and ϕ is the Bloch wave function of the thermalized positron. The integration is performed over the whole volume of the crystal and the summation is taken over the occupied electronic states. By assuming that the positron is fully thermalized, we regard **p** as the momentum of the valence electron.

The counting rate measured by the standard parallel slit apparatus is proportional to

$$\Gamma(p_x, p_y) = \int dp_z \Gamma(p_x, p_y, p_z) \tag{2}$$

We define the function $N(\mathbf{p})$ by folding $\Gamma(\mathbf{p})$ with respect to all reciprocal lattice vectors $\mathbf{G}$ as follows:

$$N(\mathbf{p}) = \sum_{\mathbf{G}} (\mathbf{p} + \mathbf{G}) \tag{3}$$

We have exactly

$$N(\mathbf{p}) = const \sum \int d\mathbf{k} \delta(\mathbf{k} - \mathbf{p} + \mathbf{G}) \frac{1}{\Omega} \int_{\Omega} |U_{n\mathbf{k}}(\mathbf{r})|^2 |V(\mathbf{r})|^2 d\mathbf{r} \tag{4}$$

Where $U_{n\mathbf{k}}$ and *V* are the periodic parts of the wave function of valence electron and positron, respectively, and the **r**-integration is performed over the unit cell with volume Ω.

In the folded function $N(\mathbf{p})$, each $\mathbf{k}$ -point in the momentum space occupied by the electrons is mapped by the δ-function in the weight of the electron-positron overlap in their densities. Corresponding to the experimental condition, $N(\mathbf{p})$ is one dimensionally integrated along the direction towards a fixed detector of γ-rays as

$$N(p_x, p_y) = \int dp_z N(p_x, p_y, p_z) \ , \tag{5}$$

the mapping of the $N(p_x, p_z)$ on the $\boldsymbol{p_x} - \boldsymbol{p_y}$ plane gives an information of the occupied $\mathbf{k}$ -space .

If the positron wave function is assumed to be constant (namely a uniform distribution of positrons), we obtain the exact geometry of the occupied $\mathbf{k}$ -space along the direction of integration, namely the projection of the first Brillouin zone, for semiconductors the real non-uniform distribution of positrons deforms the geometry, according to the weight of the electron-positron overlap .

For the calculation of the weight function, we adopted the pseudo-potential method, where the periodic parts $U_{n\mathbf{k}}$ and $V(\mathbf{r})$ are expanded in terms of the plane waves,

$$U(\mathbf{r}) = \sum_{\mathbf{R}} C_{n\mathbf{k}} \exp(i\mathbf{R}\mathbf{r}) \quad \text{for valence electrons,} \tag{6}$$

$$V(\mathbf{r}) = \sum_{G} D(\mathbf{G}) \exp(i\mathbf{G}\mathbf{r}) \quad \text{for positrons,} \tag{7}$$

Where **R**'s and **G**'s are the reciprocal lattice vectors. The weight function is expressed as follows:

$$\frac{1}{\Omega} \int |U_{n\mathbf{k}}(\mathbf{r})|^2 |V(\mathbf{r})|^2 d\mathbf{r} = \sum_{\mathbf{R'}} \sum_{\mathbf{R}} \sum_{\mathbf{G'}} \sum_{\mathbf{G}} C_{n\mathbf{k}}(\mathbf{R'}) C_{n\mathbf{k}}(\mathbf{R}) D(\mathbf{G'}) D(\mathbf{G}) \delta_{k+k'+G-G'} \tag{8}$$

the $C_{n\mathbf{k}}(\mathbf{R})'s$ and $D(\mathbf{G})'s$ were determined in the following energy band calculations .

The object of each band structure calculation, be it for an electron or a positron, is to solve the Schrödinger equation for a crystal potential *V(r),*

For the valence electrons we have

$$H\psi_{n\mathbf{k}}(\mathbf{r}) = E\psi_{n\mathbf{k}}(\mathbf{r}), \tag{9}$$

$$H = \frac{p^2}{2m} + V_{pseudo}, \tag{10}$$

where the V_{pseudo} is the empirical pseudo-potential determined by Kobayashi [19] . The form factors used in our calculations were taken from [20].

For the positron we have

$$H\phi(\mathbf{r}) = E\phi(\mathbf{r}), \tag{11}$$

$$H = \frac{p^2}{2m} + V_{\text{ionic core}} + \boldsymbol{V}_{\text{valence electrons}}, \tag{12}$$

where the $V_{\text{ionic core}}$ is the crystal ionic potential given by

$$V_{\text{ionic core}}(\mathbf{r}) = \sum_i \sum_j v(\mathbf{r} - \mathbf{R_i} - \mathbf{t_j}) \quad ; \tag{13}$$

Here, in the point core approximation we adopted

$$V(\mathbf{r}) = \frac{Ze^2}{r}, \tag{14}$$

and the potential due to the valence electrons is

$$V_{\text{valence electrons}} = -e^2 \int \frac{\rho(\mathbf{r}')d\mathbf{r}}{|\mathbf{r} - \mathbf{r}'|}. \tag{15}$$

The density of the valence electrons $\rho(\mathbf{r})$ is evaluated by using $\psi_{\boldsymbol{nk}}(\mathbf{r})$ as

$$\rho(\mathbf{r}) = 2\sum_n \sum_{\mathbf{k}} |\psi_{\mathbf{nk}}(\mathbf{r})|^2 . \tag{16}$$

The wave function of the fully thermalized positron ϕ is given, in good approximation, by the wave function $\phi_{\boldsymbol{n}=1,\boldsymbol{k}=0}$, i.e. the wave function at the bottom of the positron energy band.

The two-photon momentum density $\rho^{2\gamma}(\mathbf{p})$ for positron annihilation is given, in the IPM, by:

$$\rho^{2\gamma}(\mathbf{p}) = \sum_{n,k} \eta_n(\mathbf{k}) \left| \int d^3\mathbf{r} \exp(-i\mathbf{p}\mathbf{r}) \psi_{nk} \phi(\mathbf{r}) \right|^2 \tag{17}$$

where $\eta_{\boldsymbol{n}}(\boldsymbol{k})$ is the occupation number equal to 1 for the occupied states and zero for the empty states. For a periodic potential at zero temperature Eq. (17) will be reduced to:

$$\rho^{2\gamma}(\mathbf{p}) = \sum_{n,k} \sum_G \eta_n(\mathbf{k}) |A_{n,k}(\mathbf{G})|^2 \delta(\mathbf{p} - \mathbf{k} - \mathbf{G}) \tag{18}$$

where $A_{n,k}(\mathbf{G})$ are the Fourier coefficients of the positron-electron wave function product.

It is usual to perform a "Lock-Crisp-West" (LCW) zone folding [21] of the various extended zone components of $\rho(\mathbf{p})$ into the first Brillouin zone, thus forming the zone-reduced momentum density:

$$n(k) = \sum_{G_i} \rho(\mathbf{p} + \mathbf{G_i}) \tag{19}$$

where $\mathbf{G_i}$ is the i^{th} reciprocal lattice vector defined within the first Brillouin zone . Using Block's theorem, $\boldsymbol{n}(\boldsymbol{k})$ can be described as:

$$n(k) = const \sum_n \theta(E_F - E_{n,k}) \int |\psi_{n,k}(\mathbf{r})\phi(\mathbf{r})d\mathbf{r}|^2 \tag{20}$$

where E_F is the Fermi energy and $\theta(E_F - E_{n,k})$ is a step function as follows :

$$\theta(E_F - E_{n,k}) = \begin{cases} 1 & E_F \le E_{n,k} \\ 0 & E_F \ge E_{n,k} \end{cases} \tag{21}$$

Foe the metallic material, the two photon momentum distribution exhibits breaks at the Fermi momentum **p=k** and also another at **p=k+G**.

However, in the long slit angular correlation experiment one measures a component of the pair momentum density as given by:

$$N(p_z) = \iint \rho^{2\gamma}(\mathbf{p}) dp_x dp_y \qquad (22)$$

It contains two sets of information. The sharp breaks in $N(p_x, p_y)$ reveal the topology and size of the Fermi surface (FS) while the shape of $N(p_x, p_y)$ reflects more details of the wave functions of the electron and the positron.

The parameters used for this calculation are listed in table 1, the calculated Fourier coefficients of the valence charge densities for InN, AlN and GaN are given in table 2.

III-RESULTS

In the first step of our calculations, we have computed the Fourier coefficients of the valence charge densities using the empirical pseudopotential method (EPM) [22]. As mentioned in the introduction, this method has been proved to be largely sufficient to describe qualitatively the realistic charge densities. As input, we have introduced the form factors (the symmetric and antisymmetric parts) and the lattice constants for GaN, AlN and InN. The resulting Fourier coefficients are used to generate the corresponding positron wave function using the IPM.

The positron band structures for GaN, AlN and InN as calculated by the IPM approximation, are shown in figures 1a, 1b and 1c. the first obvious observation is the similarity between the positron and electron energy spectrum, with the exception that the positron energy spectrum does not exhibit a band gap. The lowest positron energy state is the Γ_1 state at $k_+=0$; the corresponding eigenvalue E lies several eV above the interstitial potential. The electron and positron band structures are almost free-electron like, i.e. not too far different from those we would draw for the empty lattice; the electron and the positron see the same symmetry operations, we therefore expect merely the same energy band forms. The electron and positron potentials used in our calculations are both positive, that of the positron is simply electrostatic and positive because of its charge and the absence of the exchange term. A simple electrostatic electron potential would obviously be negative, however the electron pseudopotential used here includes consideration of orthogonalization and other quantum effects, and therefore is also positive. This may explain again the similarity of the dispersion curves. The lack of energy band gap in the positron band structure is consistent with its nature.

Using the model potential and basis set described in the previous section, we computed the positron charge density at the bottom of the lowest band. These charge densities are calculated along the normal nearest-neighbor tetrahedral distance (the <111> axis) and in the $(11\bar{1})$ plane. Positron charge densities at Γ_1 for GaN, AlN and InN are displayed in figures (2) and (3a, 3b and 3c). Qualitatively, these charge distributions present nearly the same characteristics, there is however a clear buildup of positron charge distribution in the interstitial regions, and that the probability is low around the positions of the nuclei. The positron is repelled by the positively charged atomic cores and tend to move in the interstitial regions. The maximum of the charge is located at the tetrahedral site. The positron density is reduced almost to vanishing point in the immediate vicinity of the ion cores. At no point along the nearest neighbor (Ga-Al-In-N) vector is the position density more than a few percent of its peak value in the interstitial regions.

From a quantitative point of view, there is a difference of charge in the interstitial regions, the positron distribution is more pronounced in the neighborhood of the Indium (In) anion than in that of the Nitrogen (N) cation and almost the same in that of Gallium and Aluminum cation. Note the asymmetrical positron distribution in the 3 compounds, note also the difference in the positron density at the atomic cores for InN is slightly larger than that of GaN and AlN. These differences in profiles are immediately attributable to the cell which contains the larger valence and the larger ion core, due to the fact that, on one hand, Indium presents a larger valence than both Al and Ga, and on the other hand the *In* ion core is smaller than Al and Ga. We can also include the effect of the differences in the electronegativity between the elements of these alloys, the positron tends to fill the interstitial regions with ion cores having less positive charge. Consequently, we may deduce that positrons are attracted by sites with high electronic charge densities. The conclusion would be that the positron charge distribution is sensitive to the change in the valence charge density and the contribution of the core electrons results in a higher repulsion of positrons. We are considering the implications of this in regard to the propensity for positron trapping and the anisotropies that might be expected in the momentum densities for both free and trapped positron states.

We should, however, point out that the good agreement of the band structure and charge densities were used as an indication of both the convergence of our computational procedure and the correctness of the pseudopotential approach using the adjusted form factors, these latter as well as the lattice constant have been adjusted to the experimental data before the calculations.

Electron-positron momentum densities are at various occupied p=k+G. Since the contributions are continuous, thus all the bands are full, and its form can be entirely determined by the electron wave functions whose symmetries play an important role.

Figures (5 and 6) display sections of the 2D electron-positron momentum densities by integration of the appropriate plane [001] and [110] directions for InN, Aln and GaN respectively. The general feature of the observed 2D momentum distributions of annihilation radiation in InN, AlN and GaN is similar. The electron positron-positron momentum density in

the [001] directions is seen to be flat as observed in Si and Ge [23]. Compared to this, the profile along the <110> direction is sharply peaked. However, the valleys and dips observed in InN, AlN and GaN are very shallow as compared with those of Si and Ge. This fact clearly tells us that the momentum dependence is very much different between elemental and compound semiconductors.

Figures 6a, 6b and 6c display the electron-positron momentum density in the (110-001) plane GaN, AlN and InN. The features are similar for both alloys, we notice continuous contributions, i.e. there are no breaks in the distributions.

The sharp peaking along the <110> direction and the flatness of the peak along the <001> direction could also be understood in terms of the contribution of σ and π* orbitals to the ideal sp3 hybrid ones. Since the electronic configuration of Indium is $Kr4d^{10}5s^2p^1$, that of nitrogen is $2s^22p^3$, that of Aluminum is $[Ne]3s^23p^1$, and that of gallium is $Ar3d^{10}\ 4s^2\ 4p^1$, the interaction between second neighbor σ bonds is equivalent to a π antibonding interaction between neighboring atoms. Actually every σ bond interacts with three such slightly displaced, but parallel, σ bonds lying on both ends. In this case we also believe that the flattening at the top of the angular correlation annihilation radiation (ACAR) line shape along the [110] is due to the positron seeing this extra π* interaction. From the quantitative point of view, we note however, that the $e\text{-}e^+$ momentum density is more pronounced in InN than AlN and GaN, this is consistent with the electronic configurations of outer electrons in the ground atomic state as mentioned above; the reason behind this might be also due to the elemental tetrahedrally coordinated environments, the positron sees different electronic environments in the 3 compounds InN, AlN and GaN. The Indium ion cores are larger than those of Gallium and Aluminum this would lead as expected a greater positron penetration in InN than in GaN and AlN and hence a greater annihilation rate, this is manifested in the angular correlation curve as an increase in the fractional area of the broad component of the momentum. The broad component arises largely from annihilation with electrons in the ion cores which have high momentum components on their wave functions due to their localization.

Figures 7a and 7b and 7c give the calculated LCW folded distribution for InN, AlN and GaN. The momentum distribution in the extended zone scheme is represented by n(k) in the reduced zone scheme. We can deduct from the map that the electronic structure consists entirely of full valence bands, since the amplitude variation in the LCW folded data is merely constant.

The calculated electron-positron momentum density bird's eye view of reconstructed 3D momentum space density) in the (110-001) plane is displayed in Figs. 8a, 8b and 8c. There is a good agreement in the qualitative feature between our results and experimental data obtained by Berko and co-workers for carbon [24], one can notice that there is a continuous contribution, i.e. there is no break, thus all the bands are full.

Table 1: The symmetric and antisymmetric form factors (in Ry), and the lattice constant a_o (in Angstroms) for InN, AlN and GaN used in these calculations.

compound	lattice constant a_o	Experimental lattice constant a_o [20]	form factors
InN	4.98	12.2117	V_s (3) = -0.3240 V_s (8) = -0.2550 V_s (11) =0.0548 V_a (3) = 0.2090 V_a (4) =0.1740 V_a (11) =0.1790
AlN	4.36	11.5879	V_s (3) = -0.3000 V_s (8) =0.08000 V_s (11) =0.1100 V_a (3) =0.28000 V_a (4) =0.33000 V_a (11) =0.0400
GaN	4.50		V_s (3) = -0.3000 V_s (8) = -0.0600 V_s (11) =0.070 V_a (3) =0.28000 V_a (4) =0.20000 V_a (11) =0.0150

Table 2: The calculated Fourier coefficients of the valence charge densities for InN, AlN and GaN.

G($a/2\pi$)	Fourier coefficients (e/Ω)					
	InN		AlN		GaN	
000	8.00000	0.00000	8.00000	0.00000	8.00000	0.00000
111	0.107648	-0.60203	0 .19878	-0.768322	0 .21877	-0.517762
220	-0.018943	-0.02451	0.02235	-0.019876	0.02356	-0.015894
311	0.000023	-0.02333	-0.00077	-0.044761	-0.00076	-0.047861
222	0.000000	-0.28655	0.00000	-0.143354	0.00000	-0.197954
400	0.000000	0.01245	0.00000	0 .017221	0.00000	0 .016418
331	0.000654	-0.00546	0.00022	-0.000567	0.000154	-0.000654

CONCLUSION

We have performed theoretical calculations of the positronic properties of GaN, InN and AlN calculated within the pseudopotential formalism and employing the independent particle model (IPM).These distributions are found to be strongly influenced by the actual symmetry of the orbitals taking part in bonding, therefore, it is expected that the positron-annihilation technique is an effective tool and a sensitive microscopic probe of semiconductors; we have shown that by performing the electron-positron momentum densities, a deep insight into the electronic properties can be achieved. More importantly, because of its relatively few assumptions, the present theory yields a reliable single-particle description of positron annihilation. As a consequence, it represents an excellent starting point for a systematic many-particle description of the process.

ACKNOWLEDGEMENT

This work was supported by the United Arab Emirates University through the University Program for Advanced Research: 31S207-UPAR (4) 2015.

References

[1] (Vacancy defects) L. Šedivý, J. Čížek, E. Belas, R. Grill & O. Melikhova, Scientific Reports 6, Article number: 20641 (2016)

[2] S Ishibashi and A Uedono 2016 J. Phys.: Conf. Ser. 674 012020

[3] Xiaoguang Ma, , Yinghao Zhu, Yang Liu, Physics Letters A, Vol. 380, Issue 21, (2016), 1848–1855

[4] Yoyo Hinuma et al, Nature Communications 7, Article number: 11962 (2016)

[5] Zeng-Hua Cai, Prineha Narang, Harry A. Atwater, Shiyou Chen, Chun-Gang Duan, Zi-Qiang Zhu, and Jun-Hao Chu, Chem. Mater., 2015, 27 (22), pp 7757–7764

[6] Andriy Zakutayeva, J. Mater. Chem. A, 2016,4 Solid-State Electronics, 6742-6754

[7] Herbert Paul Maruska, Walden Clark Rhines, Vol. 111, (2015), 32–41.

[8] Y. Suna, J.Y. Li, Y. Tana, L. Zhanga, Journal of Alloys and Compounds 471 (2009) 400–403

[9] Steven P. DenBaars et al, Acta Materialia 61 (2013) 945–951

[10] Keun-Man Song and Jinsub Park, Semicond. Sci. Technol. (2013) 28 015010

[11] Wenbin Lv, Lai Wang, Jiaxing Wang, Yuchen Xing, Jiyuan Zheng, Di Yang, Zhibiao Hao and Yi Luo, Japanese Journal of Applied Physics, Vol. 52, Number 8S (2013)

[12] Herbert Paul Maruska, Walden Clark Rhines, Solid-State Electronics, Vol. 111, 2015, 32–41

[13] S Berrah et al 2007 Phys. Scr. 75 414

[14] S. Berrah et al, Turk J Phys 30 (2006), 513 – 518.

[15] Nan Li,a, Satyesh K. Yadav, Jian Wang,b, Xiang-Yang Liu, and Amit Misra, Sci Rep. 2015; 5: 18554.

[16] N. Amrane and Z. Mahdjoub, CHINESE JOURNAL OF PHYSICS VOL. 47, NO. 5 (2009)

[17] M. Alatalo, B. Barbiellini, M. Hakala, H. Kauppinen, T. Korhonen, M. J. Puska, K. Saarinen, Phys. Rev. B 54, 2397 – 1996

[18] P. Hautojarvi, and R. M. Nieminen, PHYSICAL REVIEW B VOLUME 54, NUMBER 4 15 JULY 1996

[19] H.Nara and T.KOBAYASHI , J.Phys.Soc.Japan 41 (1976) 1429

[20] Y. C. Yeo, T. C. Chong and M. F. Li, J. Appl. Phys. 83, 1429 (1998)

[21] D.G.Lock, V.H.C.Crisp and R.N.West, J.Phys., F3 (1973) 561.

[22] Salvador Gonzalez, Dragica Vasileska, Alexander A. Demkov, Journal of Computational Electronics, 2002, Vol. 1, Issue 1, pp 179–183

[23] K.Fujiwara, T,Hyodo, J.Phys.Soc. Jpn,35 (1973) 1133.

[24] S. Berko, M. Haghgooie, and J. J. Mader, Phys. Lett. A 63A, 335, 1977

ISSN 2347-3487
Volume 12 Number 3
Journal of Advanced Physics

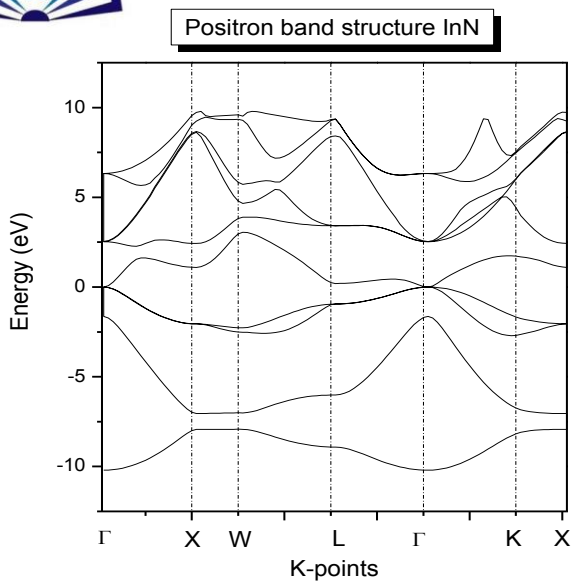

Figure 1a

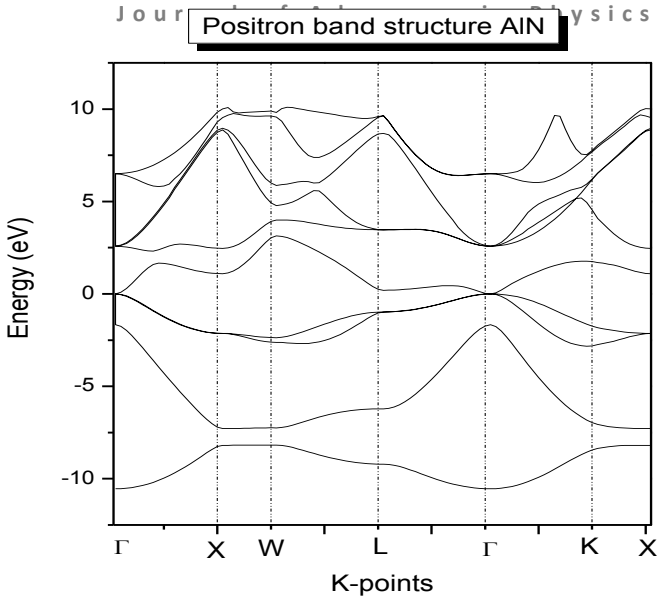

Figure 1b

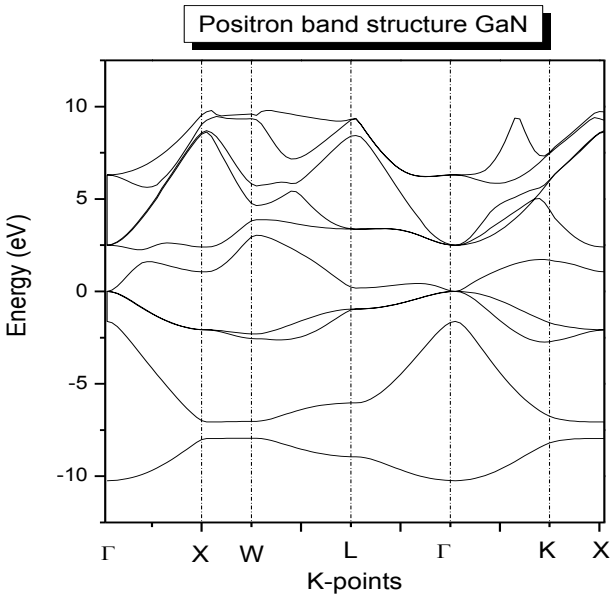

Figure 1c

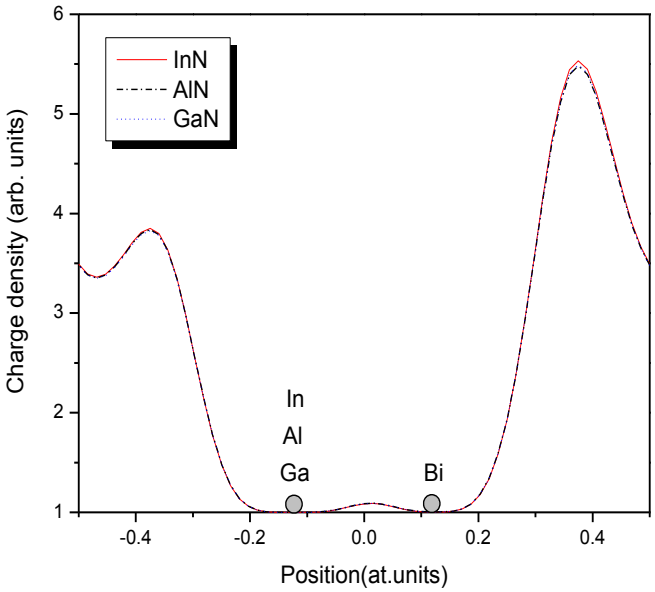

Figure 2

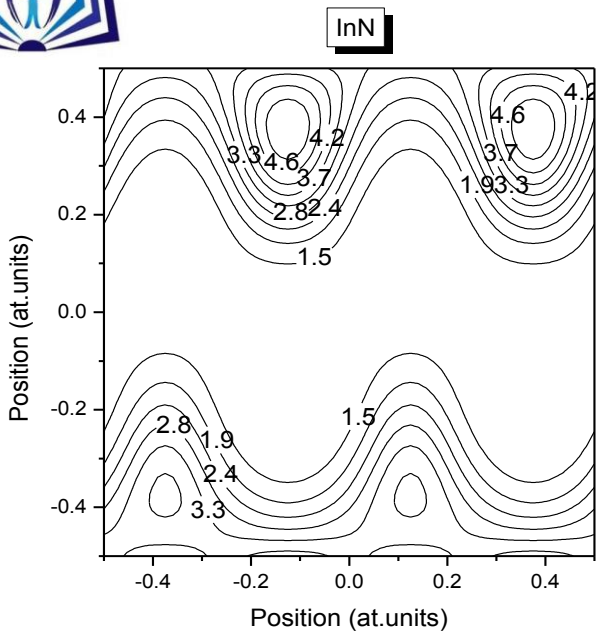

Figure 3a

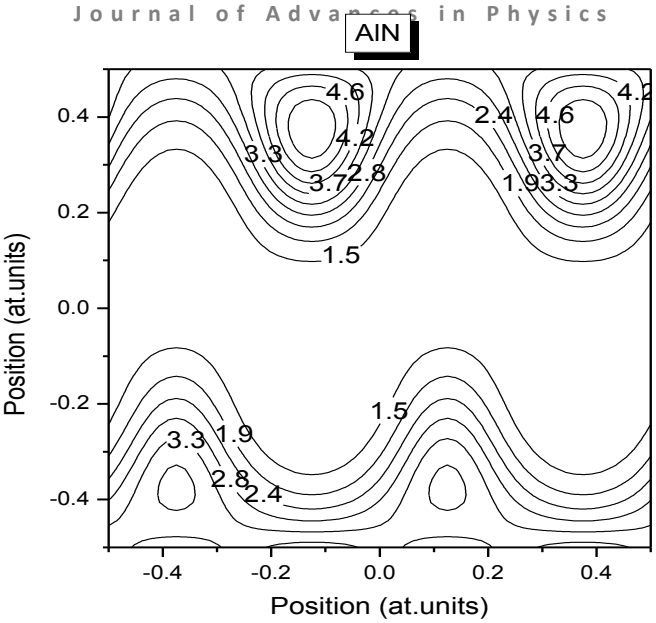

Figure 3b

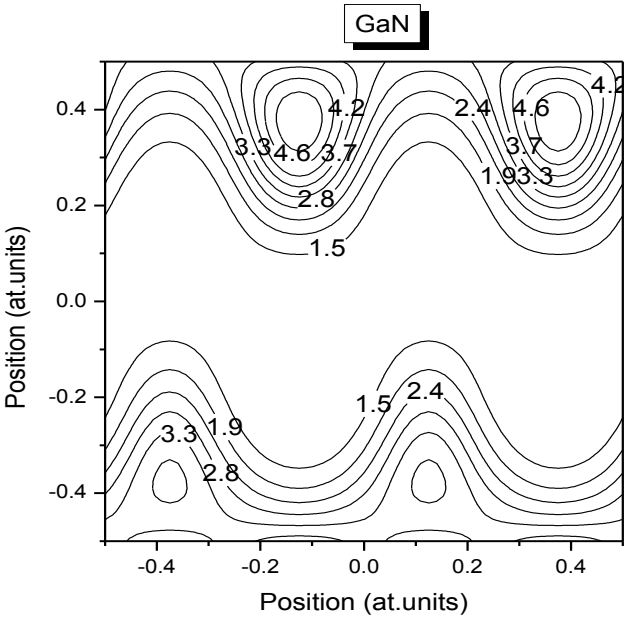

Figure 3c

ISSN 2347-3487
Volume 12 Number 3
Journal of Advances in Physics

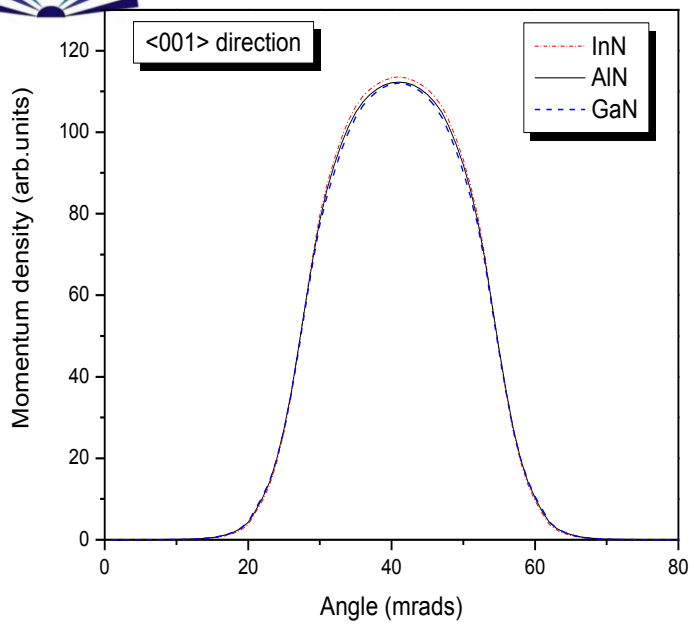

Figure 4

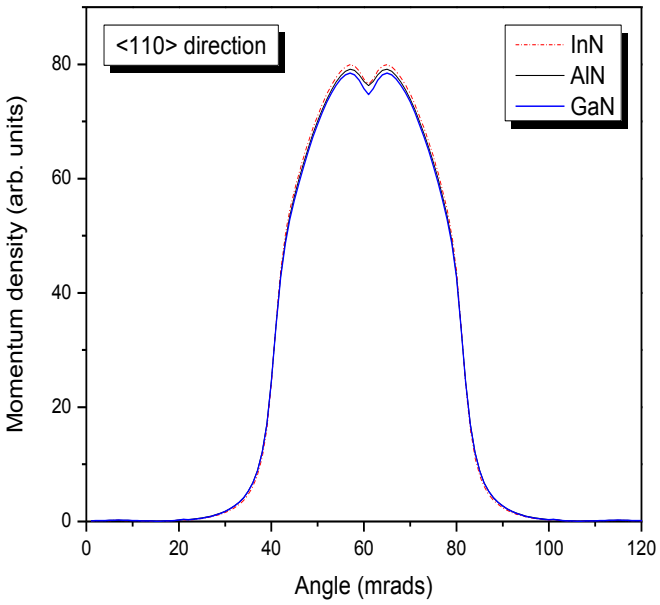

Figure 5

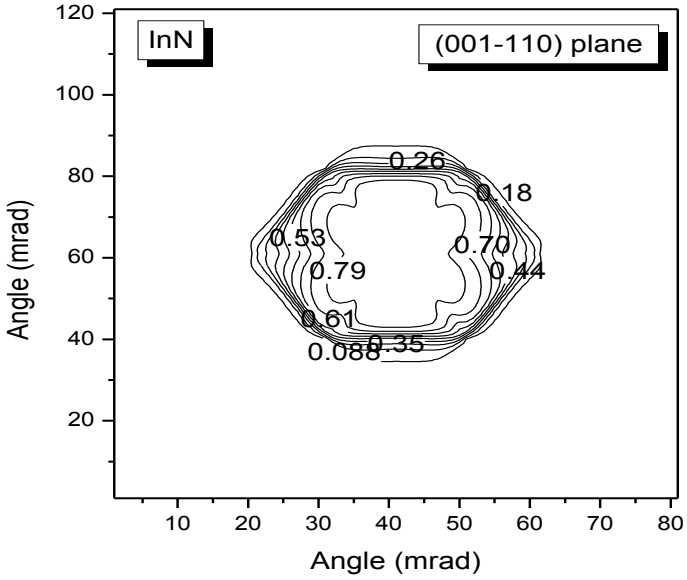

Figure 6a

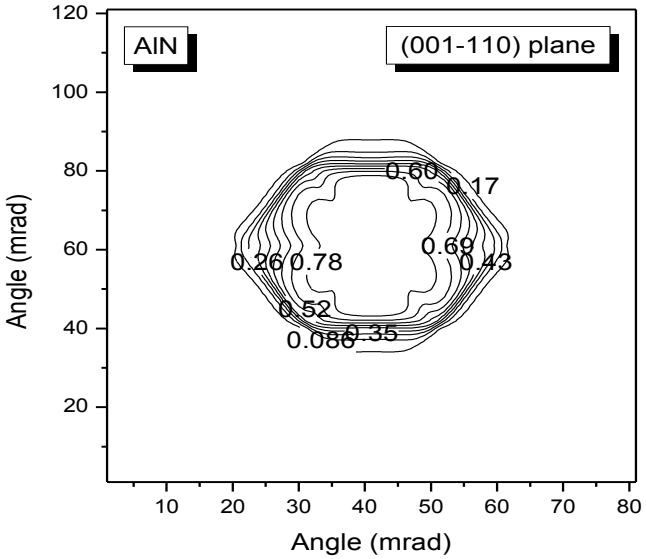

Figure 6b

ISSN 2347-3487
Volume 12 Number 3
Journal of Advances in Physics

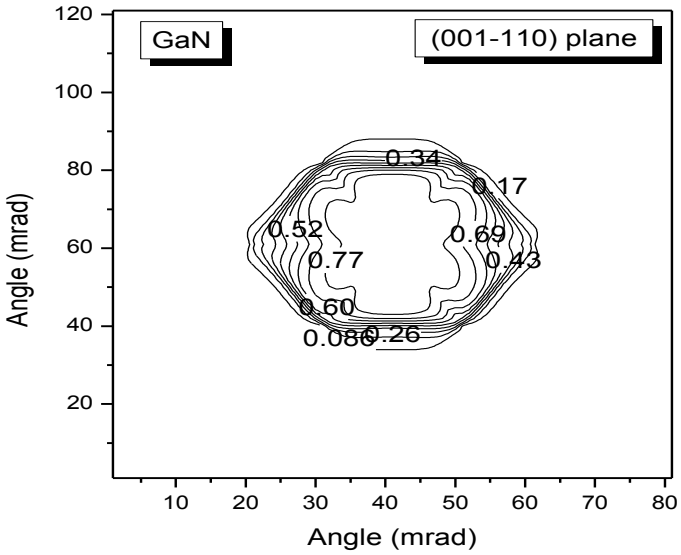

Figure 6c

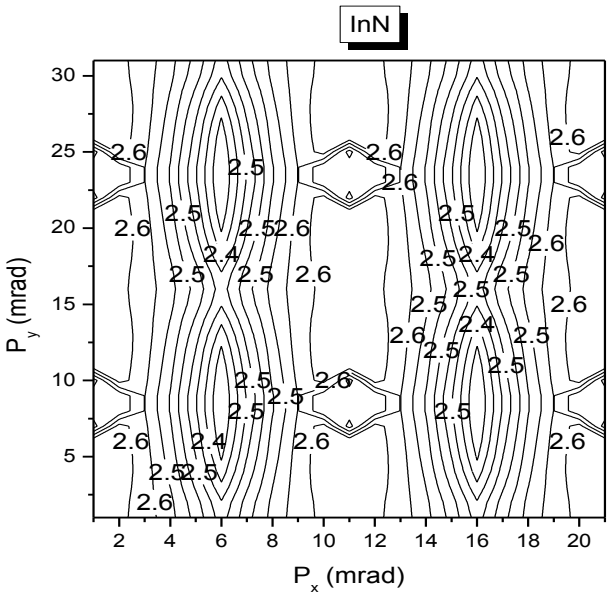

Figure 7a

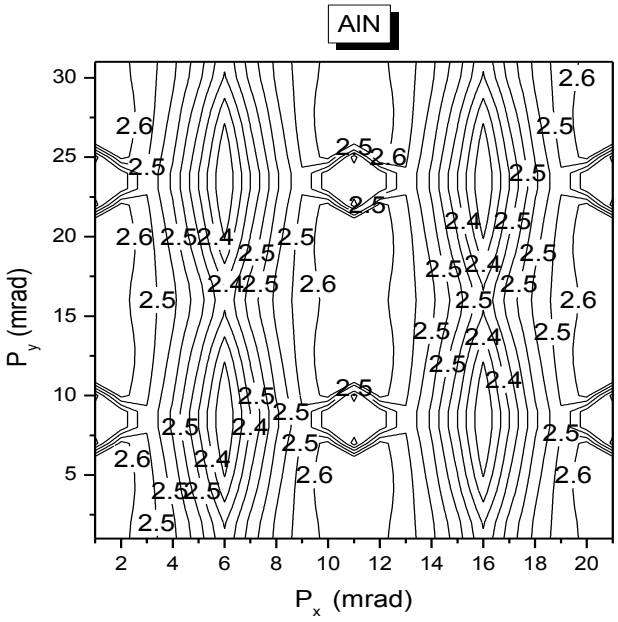

Figure 7c

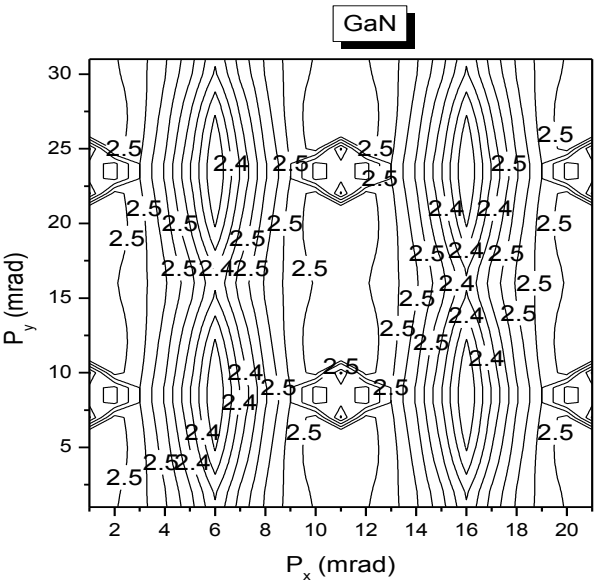

Figure 7b

ISSN 2347-3487
Volume 12 Number 3
Journal of Advances in Physics

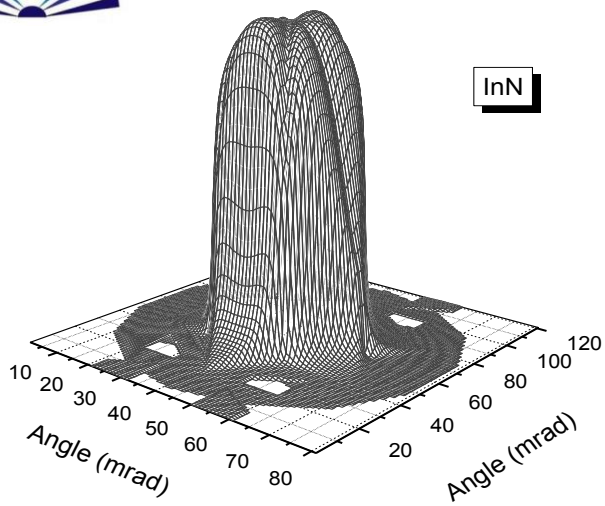

Figure 8a

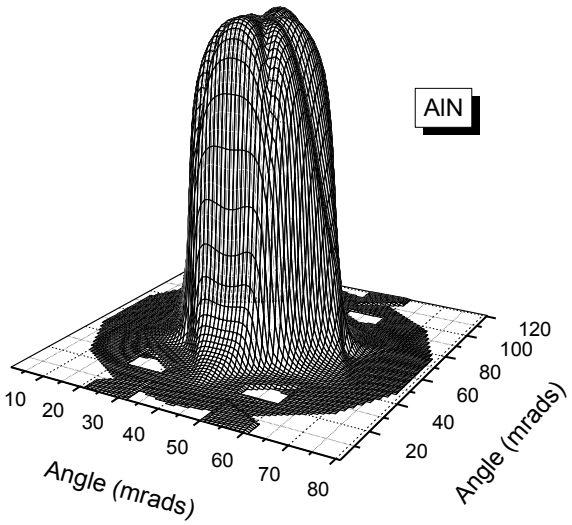

Figure 8b

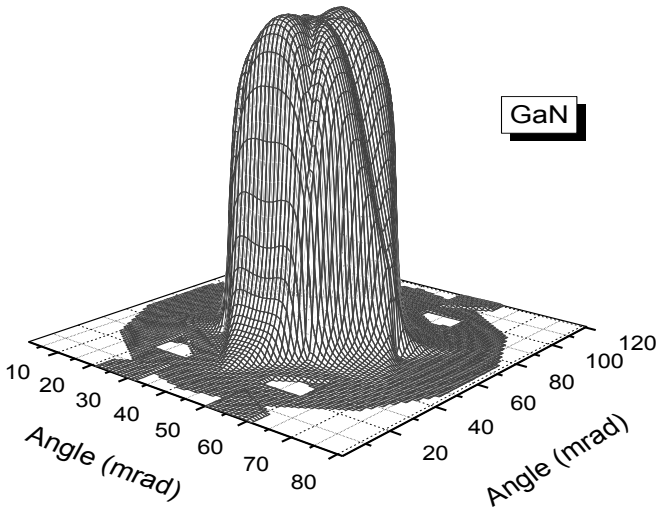

Figure 8c